SAND99-0076C

A Phase-Field Model for Grain Growth

L. Q. Chen
Department of Materials Science and Engineering
The Pennsylvania State University
University Park, PA 16802-5006

D. N. Fan and V. Tikare
Materials Modeling and Simulation
Sandia National Laboratory
Albuquerque, NM 87185-1411

July 13, 1998

Abstract

A phase-field model for grain growth is briefly described. In this model, a polycrystalline microstructure is represented by multiple structural order parameter fields whose temporal and spatial evolutions follow the time-dependent Ginzburg-Landau (TDGL) equations. Results from phase-field simulations of two-dimensional (2D) grain growth will be summarized and preliminary results on three-dimensional (3D) grain growth will be presented. The physical interpretation of the structural order parameter fields and the efficient and accurate semi-implicit Fourier spectral method for solving the TDGL equations will be briefly discussed.

Acknowledgments: This work is supported by the National Science Foundation under the grant number DMR96-33719 and by the Department of Energy/Sandia National Laboratory

1 Introduction

Computer simulation is playing an increasingly important role in the fundamental understanding of grain growth because of its ability to incorporate various levels of complexity and different types of physical processes involved in a grain growth. Many modeling approaches for grain growth have been proposed in the last decade or so. These include statistical models [1, 2, 3], vortex models [4], boundary dynamics models [5, 6], mean field models [7, 8, 9], Voronoi models [10, 11], the Potts model [12, 13, 14], the Surface Evolver [15], the Laguerre model [16, 17, 18], and models based on variational principles [19]. In spite of the different physical bases and approaches employed in these models, a common feature is the approximation of boundaries or interfaces as mathematically abstract sharp interfaces, and simulation of the grain growth process involves the explicit tracking of the interfacial positions, an exception being the Potts model.

Recently, we developed a phase-field model for studying grain growth kinetics in single-phase [20, 21, 22, 23] and two-phase materials [24, 25, 26, 27, 28]. In this model, a polycrystalline microstructure is represented by non-conserved multiple structural order parameter fields whose values are proportional to the structural amplitudes in the reciprocal space [29]. The free energy density of a grain is then formulated as a Landau expansion in terms of the structural order parameters. The grain boundary energy is introduced through the gradients of the structural order parameters. The anisotropy in grain boundary energy and mobility can be incorporated by taking into account the underlying crystalline symmetry of the grains in the free energy density function and in the gradient terms [29, 30]. The temporal and spatial evolution of the structural order parameters follow the time-dependent Ginzburg-Landau (TDGL) or Allen-Cahn equations [31] which can be solved using various numerical techniques such as finite-difference, finite-element, or spectral methods. One of the main features of the phase-field model is the fact that one does not have to explicitly track the interfaces since their are implicitly defined by the level set of the structural order parameter fields. Another distinct advantage of the phase-field model is the natural incorporation of long-range diffusion, which takes place, for example, during solute segregation at grain boundaries, by coupling the TDGL equations with the Cahn-Hilliard non-linear diffusion equation [32] for composition.

There have been many other applications of the phase-field model to modeling microstructural evolution during phase transformations and subsequent coarsening processes (see [33] for a brief overview).

The objective of this paper is to give a brief account on the theoretical background underlying the phase-field model for grain growth, and to give a brief summary on phase-field simulation results of 2D grain growth in pure systems.

2 Phase-Field Model

2.1 Representation of a Grain Structure

To understand the physical reasoning behind the phase-field representation of a microstructure, let us examine a pure solid on a simple 2D square lattice. The X-ray diffraction pattern of such a single crystal is schematically shown in Fig. 1 (left). The diffraction intensity, $I_{\mathbf{H}}$, is proportional to the square of the structural amplitude at a given point in the reciprocal

DISCLAIMER

space,Φ_H . In principle, if we know all the structural amplitudes, we have the information about the atomic structure of the crystal, i.e.

$$\rho(\mathbf{r}) = \bar{\rho}(\mathbf{r}) + \sum_H \Phi_H(\mathbf{r}) exp(i2\pi \mathbf{H}\cdot\mathbf{r}) \tag{1}$$

where $\rho(\mathbf{r})$ is the single-site occupation probability function, $\bar{\rho}(\mathbf{r})$ is the average local density, $\mathbf{H}$ the reciprocal-lattice vector corresponding to the Bravais lattice of the crystal, and $\Phi_H(\mathbf{r})$ the local structural amplitudes. According to equation (1), the structural amplitudes play the same roles as long-range order (LRO) parameters which distinguish a liquid and a solid [29]. Since there are an infinite number of LRO parameters in equation (1), such a representation is hardly useful in microstructural modeling. If we assume that the relation among the amplitudes $\Phi_H(\mathbf{r})$ are fixed at all times during a microstructural evolution, i.e.

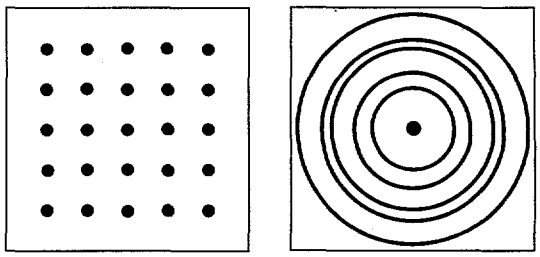

Figure 1: The schematic diffraction patterns of a square single-crystal (left) and a corresponding polycrystalline microstructure (right)

$$\Phi_H(\mathbf{r}) = \eta(\mathbf{r})\Upsilon(\mathbf{H}) \tag{2}$$

where $\eta(\mathbf{r})$ is the LRO parameter which describes the crystallinity in a given region, and $\Upsilon(\mathbf{H})$ are the constants completely determined by the symmetry in the equilibrium crystalline state. With the assumption given by equation (2), we may reduce equation (1) to a single-order parameter description, i.e.

$$\rho(\mathbf{r}) = \bar{\rho}(\mathbf{r}) + \eta(\mathbf{r})\left[\sum_H \Upsilon(\mathbf{H}) exp(i2\pi \mathbf{H}\cdot\mathbf{r})\right] \tag{3}$$

For a given crystal structure, the sum in the square bracket in equation (3) is fixed and assumed to be independent of time in our isotropic phase-model for grain growth. Although, a multicomponent order parameter is necessary in order to describe the interfacial energy anisotropy more physically [29], for the case of isotropic interfacial energies, the single LRO parameter description is sufficient.

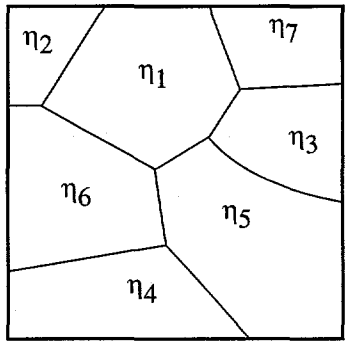

Figure 2: The schematic representation of a grain structure

The corresponding diffraction pattern of a polycrystalline grain structure is schematically shown in Fig. 1(right). We can write down an approximate expression for the single-site occupation probability density function for the polycrystalline state using the single LRO description,

$$\rho(\mathbf{r}) = \bar{\rho}(\mathbf{r}) + \sum_{i=1}^{i=Q} \eta_i(\mathbf{r})\left[\sum_H \Upsilon(\mathbf{H_i}) exp(i2\pi \mathbf{H_i}\cdot\mathbf{r})\right] \tag{4}$$

where Q is the number of crystallographic orientations of grains in a microstructure, $\mathbf{H_i}$ the reciprocal lattice vector corresponding to the *ith* crystallographic orientation, and $\eta_i(\mathbf{r})$ the LRO parameter representing the crystallinity with the *ith* orientation at position $\mathbf{r}$. Assuming homogeneous average local density, a schematic representation of a grain structure using the field LRO parameters is given in Fig. 2. Within a given grain, only one LRO parameter has a finite value while all others are zero.

2.2 Free Energy of a Grain Structure

Based on the representation discussed in the last section, the total free energy of a grain structure can be represented in a Ginzburg-Landau form as

$$F = \int_{\mathbf{r}} \left[f_{local}(\{\eta_i(\mathbf{r})\}) + \frac{1}{2}\kappa \sum_i \nabla^2 \eta_i(\mathbf{r}) \right] d^3\mathbf{r} \tag{5}$$

where the local part of the free energy, f_{local} can be expressed as a Landau expansion in terms of the LRO parameters η_i, and κ is the gradient energy coefficient. In expression (5), isotropic interfacial energy is implicitly assumed. For a more detailed discussion on the free energy formulation, including the introduction of anisotropic interfacial energies, please see reference [29] and [30]

2.3 Evolution Equations for LRO Parameters

For modeling grain structure evolution, the LRO parameters are not only space-dependent but also time-dependent. Assuming that the average local density is uniform, the LRO parameters are non-conserved fields whose evolution follows the traditional Ginzburg-Landau equation or Allen-Cahn equation,

$$\frac{\partial \eta_i}{\partial t} = -L\left(\frac{\delta F}{\delta \eta_i}\right) \tag{6}$$

where L is a kinetic coefficient related to interface mobility, t is time, $1 \leq i \leq Q$, and

$$\frac{\delta F}{\delta \eta_i} = \frac{\partial f_{local}}{\partial \eta_i} - \kappa \nabla^2 \eta_i \tag{7}$$

In a grain growth simulation, the systems of equations (6) are numerically solved.

2.4 Sharp-Interface Limit

To relate the kinetic coefficient L and the gradient energy coefficient κ to familiar quantities controlling grain growth such as grain boundary energy and mobility, let us examine the correspondent sharp-interface limit of the phase-field equations for the simple case of a circular grain in 2D and a spherical grain in 3D embedded in another grain. In the conventional theory, it is easy to show that the radius of a circular or a spherical grain, R, will decease according to

$$R^2 - R_o^2 = \begin{cases} -2M_{gb}\gamma_{gb}\Omega t & \text{for a circular grain} \\ -4M_{gb}\gamma_{gb}\Omega t & \text{for a spherical grain} \end{cases} \tag{8}$$

where R_o is the radius of a circle or a sphere at $t = 0$. In the limit that the radius of the circle is much larger than the interfacial thickness, the corresponding equations from the TDGL equation are

$$R^2 - R_o^2 = \begin{cases} -2L\kappa t & \text{for a circular grain} \\ -4L\kappa t & \text{for a spherical grain} \end{cases} \tag{9}$$

Therefore, the term, $M_{gb}\gamma_{gb}\Omega$ in the conventional grain growth theory is modeled by the product of kinetic coefficient L and the gradient energy coefficient κ in phase-field simulations.

2.5 Numerical Solution to Evolution Equation

The simplest technique to solve the phase-field equations is to combine the explicit forward Euler method in time and the finite-difference method in space. For example, in 2D, the Laplacian operator in (7) at a given time step n is usually discretized by using a second-order five-point finite-difference approximation,

$$\nabla_h^2 \eta_i^n = \frac{1}{(\Delta x)^2} \sum_j (\eta_j^n - \eta_i^n) \tag{10}$$

where $h = \Delta x$ is the spatial grid size and j represents the set of first nearest neighbors of i in a square grid. The explicit Euler finite-difference scheme can then be written as

$$\eta_i^{n+1} = \eta_i^n + \Delta t \left[(f(\eta^n))_i + \nabla_h^2 \eta_i^n \right] \tag{11}$$

where Δt is the time step size. The above scheme is the most often used scheme in numerical simulations of the TDGL or Cahn-Hilliard equations. However, to maintain the stability and to achieve high accuracy for the solutions, the time step and spatial grid size have to be very small, which seriously limits the system size and time duration of a simulation.

Recently, Chen and Shen developed an accurate and efficient semi-implicit Fourier-spectral method for solving the phase-field equations [34]. For instance, a second-order backward difference (BDF) for $\frac{d}{dt}\tilde{\eta}$ and a second-order Adams-Bashforth (AB) for the explicit treatment of nonlinear term lead to the following second-order BDF/AB scheme:

$$(3 + 2\Delta t k^2)\tilde{\eta}^{n+1}(\mathbf{k}) = 4\tilde{\eta}^n(\mathbf{k}) - \tilde{\eta}^{n-1}(\mathbf{k}) + 2\Delta t \left[2\{\tilde{f}(\eta^n)\}_\mathbf{k} - \{\tilde{f}(\eta^{n-1})\}_\mathbf{k} \right]. \tag{12}$$

where $\mathbf{k} = (k_1, k_2)$ is a vector in the Fourier space, $k = \sqrt{k_1^2 + k_2^2}$ is the magnitude of $\mathbf{k}$, $\tilde{\eta}(\mathbf{k}, t)$ and $\{\tilde{f}(\eta)\}_\mathbf{k}$ represent the Fourier transforms of $\eta(x, t)$ and $f(\eta)$, respectively. Spectral methods are widely used in fluid dynamics [35]. Due to the exponential convergence of the Fourier-spectral discretization for the space-derivatives, this method requires a significantly smaller number of grid points to resolve the solution to within a high prescribed accuracy than the conventional finite-difference method. The second-order semi-implicit treatment in time enables one to use considerably larger time step size while maintaining stability. Another potentially powerful numerical technique to solve the phase-field equations is to use the adaptive grid method [36].

3 Grain Growth Simulations

3.1 Local free energy density function

For the purpose of modeling grain growth in a pure system, we assume the following simple local free energy density function [20, 21, 22, 23]

$$f(\eta_1, \eta_2, \cdots, \eta_Q) = \sum_{i=1}^{Q} \left(-\frac{A}{2}\eta_i^2 + \frac{B}{4}\eta_i^4 \right) + C \sum_{i=1}^{Q} \sum_{j \neq i}^{Q} \eta_i^2 \eta_j^2 \tag{13}$$

where A, B, and C are positive constants. Q represents the number of grain orientations in a grain structure. Although the exact form of the free energy density function is important

in describing the thermodynamic nature of a liquid→solid transformation, it is not very important for the motion of grain boundaries as one can see from equation (9). It may be shown that if $C > \frac{B}{2}$, the local free energy function (13) has $2Q$ minima located at

$$(\eta_1, \eta_2, \cdots, \eta_Q) = (1, 0, \cdots, 0), (0, 1, \cdots, 0), \ldots, (0, 0, \cdots, 1), etc.$$

In modeling grain growth, each of the $2Q$ minima represents a specific crystallographic orientation of grains.

3.2 Migration of a spherical grain boundary

To check the accuracies of the numerical solutions of the phase-field equations, we studied the migration of a spherical grain boundary by choosing the following numerical values: $A = 1.0, B = 1.0, C = 1.0, \kappa = 2.0, L = 1.0$. The TDGL phase-field equations were solved using the second-order semi-implicit Fourier-Spectral method (SIFSM2nd) with $\Delta x = 2.0$ and $\Delta t = 0.5$. The dependence of the grain radius squared vs. t is plotted in Fig. 4 which shows a linear dependence, in agreement with the prediction from conventional theories on curvature-driven grain boundary migration. The analytical solution (equation (9)) obtained by assuming that the grain radius is much larger than the boundary thickness is also shown in Fig. 4. It appears that with an accurate numerical technique, the grain boundary migration kinetics obtained in a numerical simulation can match very well with the analytical solution on the sharp-interface limit (error in the slope $\approx 0.04\%$).

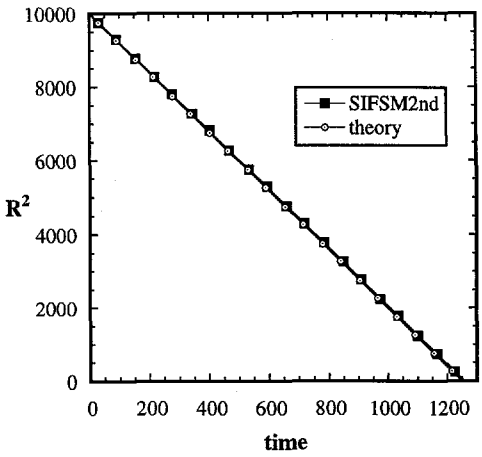

Figure 3: Dependence of R^2 on time t where R is the radius of a spherical grain

3.3 2D grain growth

We have performed extensive simulations on 2D grain growth using the continuum phase-field model[20, 21, 22, 23]. We have applied both the finite-difference forward Euler technique and the second-order semi-implicit Fourier-spectral method. The two numerical techniques produced very similar results on the microstructure, the growth exponent, the particle size and topological distributions, but quite different values for the rate constants in the grain growth law due to their differences in the numerical accuracies. Assuming $A = 1.0$, $B = 1.0$, $C = 1.0$, $\kappa = 2.0$, $L = 1.0$, $\Delta x = 2.0$, $\Delta t = 0.25$ and periodic boundary conditions, an example of microstructural evolution obtained from a finite-difference method is shown in Fig. 4. The computational cell size is 512×512 and $Q = 36$. The initial condition is specified by assigning small random values to all field variables at every grid point, e.g., $-0.001 < \eta_i < 0.001$, simulating a liquid. The gray-levels represent the value of $\sum_{i=1}^{Q} \eta_i^2$ with black and white corresponding to low and high values respectively.

Due to the limitation on the manuscript length, we will summarize our main results on 2D grain growth obtained from the continuum phase-field model[22, 23]:

- Grain growth in 2D follows the growth law, $R^m - R_o^m = kt$ with the exponent $m = 2$ and independent of Q. Recently, Mullins [37] introduced a constant β in his curvature-driven grain growth model with uniform boundaries as defined in $R^2 - R_o^2 = 2\beta M_{gb}\gamma_{gb}t$.

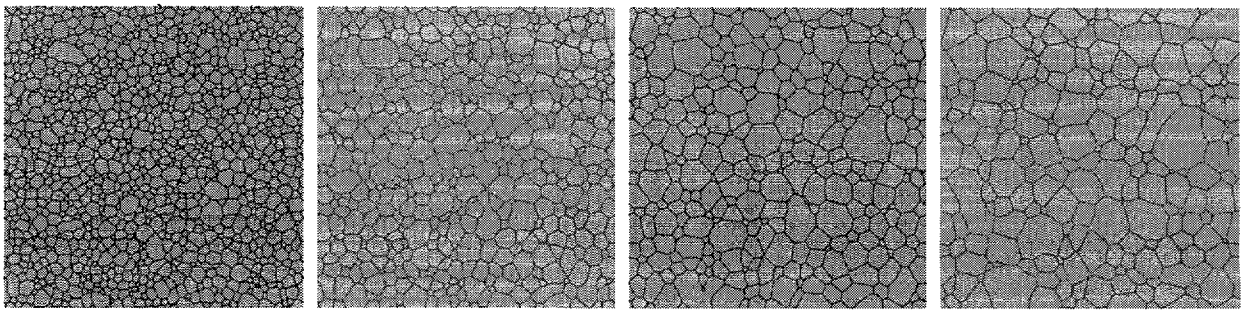

$t = 250$ $t = 750$ $t = 1250$ $t = 2000$

Figure 4: Temporal microstructural evolution during a 2D grain growth obtained using the phase-field model with 512×512 grid points and $Q = 36$

The β values obtained in our phase-field simulations using the Semi-Implicit Fourier-Spectral method are listed in Table 1. In our phase-field simulations, it is shown that the value of β depends on Q at small Q, and it is around $0.19 - 0.20$ at large Q appropriate for grain growth. A similar value for β was found in Potts model simulations of 2D grain growth [38]. A more detailed test of Mullins' theory using the continuum phase-field model will be published elsewhere.

Table 1. The constant β in Mullins' theory as a function of Q

Q	18	36	54	72	90	108	144	180
β	0.289	0.240	0.229	0.211	0.194	0.194	0.196	0.205

- The grain size distributions obtained in our 2-D simulation are shown to fit reasonably well to the Louat's function [39], $F(x) = 2ax\exp(-ax^2)$, where $x = \log(\frac{R}{\bar{R}})$ and a is an adjustable parameter, but not as well to the log-normal distribution, $F(x) = \frac{1}{\sqrt{2\pi\sigma^2}}\exp\left(\frac{-(x-x\ )^2}{2\sigma^2}\right)$, where x_o is the mean of x, and σ is the standard deviation of the distribution.

- Mullins-Von Neumann law [40, 41], $\frac{dA}{dt} \propto (n-6)$, is found to hold on the average.

- Contrary to the general belief that 4- and 5-sided grains have to transform to 3-sided before their disappearance in 2-D grain growth, phase-field simulations show evidence that 4-sided and 5-sided grains may transform to a disordered region and directly vanish.

- The shape distribution is time-invariant and the peak is found at $n = 5$, where n is number of sides, consistent with experimental results [42, 14] and Potts model simulations [13, 14], but different from the simulations based on the mean field theories [42, 7] which predicted the peak at $n = 6$.

- The second moment of the shape distribution $= 2.3 - 2.4$ is close to that obtained in Potts model simulations [14] and metallic films [42].

- The correlation between the number of sides n of a grain and the average sides of its neighbors, $m(n)$ is found to obey the Aboav-Weaire law [43, 44], $m(n) = 6 - a + \frac{6a+\mu_2}{n}$ where μ_2 is the second moment of the side distribution and a is a constant with its value close to unity.

- Although the phase-field simulation results do not follow the Lewis law [45], $\langle A_n \rangle = a(n - n_o)$ where $\langle A_n \rangle$ is the average area of n-sided grains at a given time, a and

n_o are constants dependent on the properties of the grain structure, but the data fit quite well to the Feltham law [46], $\langle R_n \rangle = a'(n - n'_o)$ where $\langle R_n \rangle$ is the average grain radius of n-sided grains, and a' and n'_o are constants.

3.4 3D grain growth

We have carried out preliminary 3D grain growth simulations using the continuum phase-field model. We employed the same set of parameters as 2D simulations and solved the evolution equations using a finite-difference method with a grid size $\Delta x = 2.0$ and a time step $\Delta t = 0.2$. An example of microstructural evolution obtained 2D cuts of 3D simulated grain structures is shown in Fig. 5. The computational cell size is $128 \times 128 \times 128$ and $Q = 54$. The initial condition for the structural LRO parameter fields corresponds to a liquid. Therefore, the initial stage during the annealing involves crystallization of a quenched liquid. The microstructure at $t = 20$ is actually a partially crystallized solid-liquid two-phase mixture. After the system is fully crystallized, grain growth takes place, resulting in the increase in grain size. The average area as a function of time obtained from the 2D cross-sections during grain growth is plotted in Fig. 6, which also shows a linear relationship as in 2D. Therefore, grain growth in 2D and 3D appear to have the same growth exponent. The detailed comparisons between results obtained from 2D simulations and those obtained from 2D cross-sections of 3D microstructures will be presented elsewhere due to space limitations.

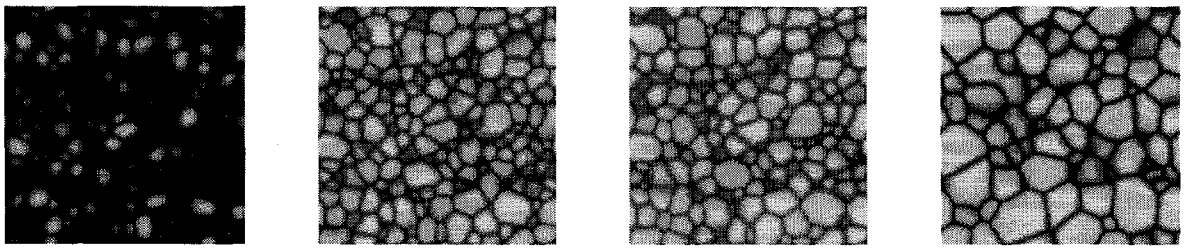

$t = 20$ $t = 40$ $t = 60$ $t = 200$

Figure 5: Temporal evolution on 2D cross-sections of 3D grain structures obtained using the phase-field model with $128 \times 128 \times 128$ grid points and $Q = 54$.

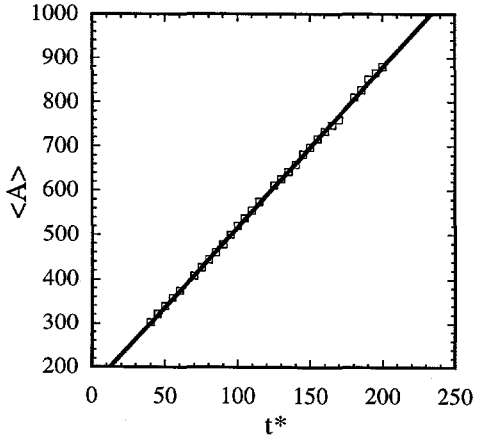

Figure 6: The average area as a function of time obtained from 2D cross-sections of 3D simulated grain structures using the continuum phase-field model

4 Summary

It is shown that the continuum phase-field model is based on a rather solid physical background and is a powerful simulation tool for studying grain growth. The results briefly discussed in the paper are all concerned with grain growth in pure systems. The real power of the phase-field model is its ability to incorporate the long-range diffusion in a rather natural way, and hence it is particularly suitable for studying diffusion-controlled microstructural evolution processes (see for example, [24, 25, 26, 27, 28]).

References

[1] N. Rivier. *Phil. Mag. B*, 52:795, 1985.

[2] W. W. Mullins. *Scripta metall.*, 22:1441, 1988.

[3] R. M. C. de Almeida and J. R. Iglesias. *J. Phys. A*, 21:3365, 1988.

[4] K. Kawasaki, T. Nagai, and K. Nakashima. *Phil. Mag. B*, 60:399, 1989.

[5] D. Weaire, F. Bolton, P. Molho, and J. A. Glazier. *J. Phys.: Condense Matter*, 3:2101, 1991.

[6] D. Weaire and H. Lei. *Phi.l Mag. Lett.*, 62:427, 1990.

[7] C. W. J. Beenakker. *Phys. Rev. A*, 37:1697, 1988.

[8] M. Marder. *Phys. Rev. A*, 36:438, 1987.

[9] C. V. Thompson, H. J. Frost, and F. Spaepen. *Acta metall.*, 35:887, 1987.

[10] S. Kumar, S. K. Kurtz, J. R. Banavar, and M. G. Sharma. *J. Stat. Phys.*, 67:523, 1992.

[11] S. K. Kurtz and F. M. A. Carpay. *J. Appl. Phys.*, 51:5125, 1980.

[12] M. P. Anderson, D. J. Srolovitz, G. S. Grest, and P. S. Sahni. *Acta metall.*, 32:783, 1984.

[13] D. J. Srolovitz, M. P. Anderson, P. S. Sahni, and G. S. Grest. *Acta metall.*, 32:793, 1984.

[14] J. A. Glazier. *Phil Mag. B*, 62:615, 1990.

[15] K. Marthinsen, O. Hunderi, and N. Ryum. In L. Q. Chen et al., editors, *Mathematics of Microstructure Evolution*, number 17 in All ACM Conferences, pages 15–22, Warrendale, PA, 1996. TMS.

[16] H. Telley, Th. M. Liebling, and A. Mocellin. *Phil Mag. B*, 73:395, 1996.

[17] H. Telley, Th. M. Liebling, and A. Mocellin. *Phil Mag. B*, 73:409, 1996.

[18] X. Xue, F. Righetti, T. M. Liebling H. Telley, and A. Mocellin. *Phil Mag. B*, 75:567, 1997.

[19] S. P. A. Gill and A. C. F. Cocks. *Acta metall.*, 44:4777, 1996.

[20] L. Q. Chen. *Scripta metall. et mater.*, 32:115, 1995.

[21] L. Q. Chen. *Phys. Rev. B*, 50:15752, 1994.

[22] D. N. Fan and L. Q. Chen. *Acta mater.*, 45:611, 1997.

[23] D. N. Fan and L. Q. Chen. *Acta mater.*, 45:1115, 1997.

[24] L. Q. Chen and D. N. Fan. *J. of Am. Ceram. Soc.*, 79:1163, 1996.

[25] D. N. Fan and L. Q. Chen. *J. Am. Ceram. Soc.*, 89:1773, 1997.

[26] D. N. Fan and L. Q. Chen. *Acta mater.*, 45:4145, 1997.

[27] D. N. Fan, L. Q. Chen, and S. P. Chen. *J. Am. Ceram. Soc.*, 81:526, 1998.

[28] D. N. Fan, L. Q. Chen, S. P. Chen, and P. W. Voorhees. *Comp. Mater. Sci.*, 9:329, 1998.

[29] A. G. Khachaturyan. *Phil. Mag. A*, 74:3, 1996.

[30] M. Venkitachalam, L. Q. Chen, A. G. Khachaturyan, and G. L. Messing. *Mater. Sci. and Eng. A*, 238:94, 1997.

[31] S. M. Allen and J. W. Cahn. *Acta metall.*, 27:1085, 1979.

[32] J. W. Cahn. *Acta Metall.*, 9:795, 1961.

[33] L. Q. Chen and Y. Z. Wang. *Journal of Metals*, 48:11, 1996.

[34] L. Q. Chen and J. Shen. *Comp. Phys. Comm.*, 108:147, 1998.

[35] Claudio Canuto et al., editors. *Spectral Methods in Fluid Dynamics.* Springer series in computational physics. Springer-Verlag, New York, 1988.

[36] N. Provatas, N. Goldenfeld, and J. Dantzig. *Phys. Rev. Lett.*, 80:3308, 1998.

[37] W. W. Mullins. Submitted to Acta mater., 1998.

[38] A. D. Rollet. Unpublished, 1998.

[39] N. P. Louat. *Acta metall.*, 22:721, 1974.

[40] W. W. Mullins. *J. Appl. Phys.*, 27:900, 1956.

[41] J. von Newmann. *Metals Interfaces*, pages 108–110. Am. Soc. for Metals, Cleveland, 1952.

[42] V. E. Fradcov, L. S. Shvindlerman, and D. G. Udler. *Scripta metall.*, 19:1285, 1985.

[43] D. A. Aboav. *Metallography*, 3:383, 1970.

[44] D. Weaire. *Metallography*, 7:157, 1974.

[45] D. Lewis. *Anat. Rec.*, 38:351, 1928.

[46] P. Feltham. *Acta mater.*, 5:97, 1957.